Current Optics and Photonics
Vol. 3, No. 5, October 2019, pp. 438-444

ISSN: 2508-7266(Print) / ISSN: 2508-7274(Online)
DOI: https://doi.org/10.3807/COPP.2019.3.5.438

Wideband Slow Light in a Line-defect Annular Photonic-crystal Waveguide

Feng Kuang[1], Feng Li[2], Zhihong Yang[2]*, and Hong Wu[2]*

[1]College of Electronic and Optical Engineering & College of Microelectronics, Nanjing University of Posts and Telecommunications (NJUPT), Nanjing 210023, China
[2]New Energy Technology Engineering Laboratory of Jiangsu Province & School of Science, Nanjing University of Posts and Telecommunications (NJUPT), Nanjing 210023, China

(Received May 2, 2019 : revised July 15, 2019 : accepted July 27, 2019)

In this theoretical study, a line-defect photonic-crystal waveguide hosted in an annular photonic crystal was demonstrated to provide high-performance slow light with a wide band, low group-velocity dispersion, and a large normalized delay-bandwidth product. Combined with structural-parameter optimization and selective optofluid injection, the normalized delay-bandwidth product could be enhanced to a large value of 0.502 with a wide bandwidth of 58.4 nm in the optical-communication window, for a silicon-on-insulator structure. In addition, the group-velocity dispersion is on the order of 10^5 (ps^2/km) in the slow-light region, which could be neglected while keeping the signal transmission unchanged.

Keywords : Annular photonic crystals, Slow light, Normalized delay-bandwidth product
OCIS codes : (130.5296) Photonic crystal waveguides; (230.5298) Photonic crystals; (260.2030) Dispersion

I. INTRODUCTION

In recent years, slow light in photonic-crystal waveguides (PCWs) has attracted much attention, since the effect remains excellent at room temperature and corresponding devices can be fabricated using traditional semiconductor technologies, providing many potential advantages in signal processing, optical storage [1], tunable delay [2], modulator and filter [3-5]. Generally a PCW is obtained by introducing a line defect into a perfect PC structure, which results in waveguide modes within the photonic band gap of the host PC and excites slow light near the Brillouin zone's edges. The slow-light performance parameters of the PCWs to which attention is usually paid are the group index n_g and the bandwidth $\Delta\omega$. However, there is interaction between the group index and bandwidth, increasing the former results in decrease of the latter [6]. The method of solving this conflict involves the idea of obtaining flat bands on dispersion curves by locally modifying the effective index in the surroundings of the PCWs, which can be achieved by varying the radius or position of the PC air holes adjacent to the waveguide's center [7-10], or by selective optofluidic filling of the structure [11-14].

An annular photonic crystal (APC) [15] is an unusual type of PC structure composed of a two-dimensional (2D) lattice of annular dielectric rods in air, or annular air voids in a dielectric background. This structure has been proposed to achieve a large absolute band gap [16], polarization-independent slow light [17], and polarization beam splitting [18]. Because it is a composite unit, an APC presents more possibilities than a normal PC in dispersion engineering. Therefore, in this research we chose an APC as the host of the PCWs, to explore the possibility of obtaining flat-band slow light. Combined with structural-parameter modification and selective optofluidic injection, optimized APCWs can support high-performance slow light with a constant group index, broad bandwidth, and low group-velocity dispersion.

II. STRUCTURE AND DISCUSSION

Inspired by reference 16, we designed an APC slab

*Corresponding author: yangzhihong@njupt.edu.cn, ORCID 0000-0003-3013-7932
wuhong@njupt.edu.cn, ORCID 0000-0002-5773-7164

Color versions of one or more of the figures in this paper are available online.

based on a triangular lattice above a SiO_2 layer with a refractive index of 1.45. The remaining portion within the slab was silicon (Si) with a refractive index $n_{Si} = 3.4$, and the slab thickness was 220 nm. Figure 1 shows the two-dimensional *x*-*z* spatial distribution of the proposed APC structure. The inner and outer radii of the annuli in the figure are denoted by r and R respectively. According to [16], it has been proven that for low air-volume filling factors around 15%, APC slabs can exhibit a significantly larger photonic bandgap (PBG) than conventional PC slabs. A large PBG is unquestionably very important for obtaining broadband slow light. Therefore, we set $R = 0.32a$ and $r = 0.21a$, and the corresponding air-volume filling factor was 20%.

To save calculation time, it was necessary to calculate the dispersion properties of the APC slabs using a 2D simulation instead of a 3D simulation. As 2D approximation methods, the effective-index method [19, 20] and effective-period method [12, 21] have been successfully applied to the design of PC devices. Especially in Ref. [21], the latter method was shown to provide more accurate estimation of device behavior than the former. Therefore, we utilized 2D simulations by means of the effective-period method. In this method, the 2D effective period for our structure was calculated to be $a_{eff} = \frac{n_{eff}}{n_{Si}} a$, where n_{eff} is the fundamental-mode effective index of the ideal multilayer slab waveguide, for a wavelength of 1550 nm. We took the lattice constant to be $a = 480$ nm, and the effective index to be $n_{eff} = 2.835$. Then the effective period was calculated to be $a_{eff} = 400$ nm. Using the 2D plane-wave-expansion (PWE) method, a broad PBG for the transverse electric (TE) polarization lay between the normalized frequencies 0.254 ($2\pi c/a$) and 0.314 ($2\pi c/a$) for $R = 0.32a$ and $r = 0.21a$. It is worth mentioning that the PBG here matched very well the PBG obtained by the 3D PWE method in Ref. [16] for an APC with the same structural parameters. This proved that the 2D method can accurately model 3D APC slabs with low AVFs.

A line-defect APC waveguide with $w = \sqrt{3}\,a$ as formed by removing a row of annuli in the *x*-direction. The corresponding band structure for the APCW in the *x*-direction for TE polarization is shown in Fig. 2(a). In the figure, the light line for SiO_2 is depicted with a dotted blue line, and the odd and even modes are represented by dotted black and solid green curves respectively. In a realistic structure based on a slab waveguide, out-of-plane losses can be considerable, but we focused only on the region of interest in reciprocal space where the APCW mode remained under the light line, thus mitigating such losses. Moreover, since the even modes couple dominantly to the incident external optical field in typical applications, all the following discussions will focus on the even modes only. The group index (defined as $n_g = c/v_g$, where c is the speed of light in vacuum) corresponding to the even

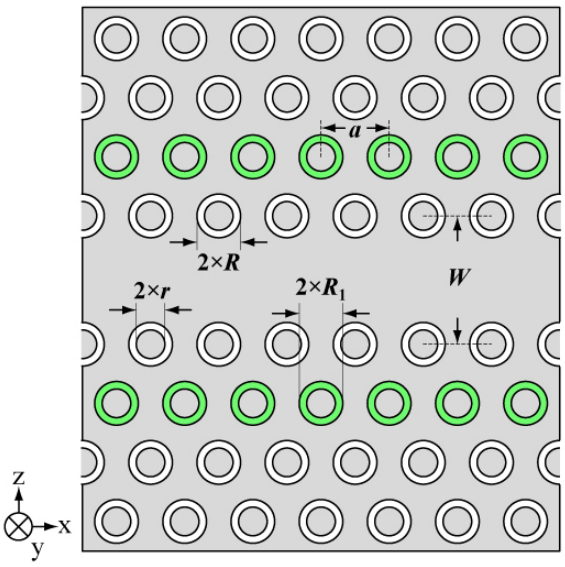

FIG. 1. A schematic of the line-defect waveguide with APC structure: r denotes the inner radius of all annular air holes; R_1 denotes the outer radius of the second row of the annular air holes adjacent to the line defect; and R indicates the outer radius of the other annular air holes.

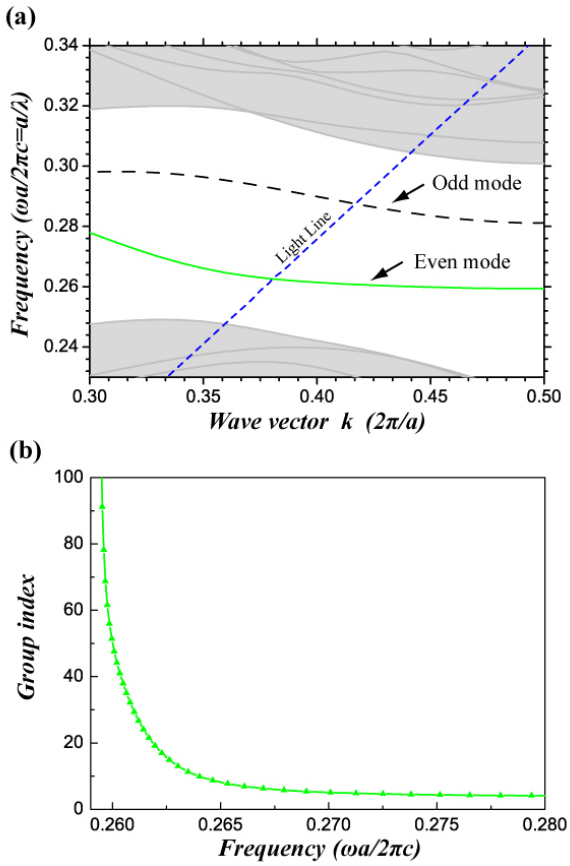

FIG. 2. (a) Dispersion curve for the original APCW with an effective lattice constant of $a_{eff} = 400$ nm. (b) The group-index curve for the even mode in (a).

mode is shown in Fig. 2(b). The group velocity v_g is the first derivative of the APCW dispersion, *i.e.* $v_g = |\partial\omega/\partial k|$. Evidently the group index decreased very rapidly with increasing frequency, which means that such a waveguide mode could not provide a constant group index with a wide bandwidth. The way to eliminate this problem was to obtain flat bands from the dispersion curves.

Based on previous work, some parameters are known to influence the dispersion, to obtain polarization-independent waveguiding and slow light in 2D APCWs [17, 22]. Such parameters include the radii and positions of the first two rows of the annuli, the width of the waveguide, and so on. To achieve a flat band, we altered the outer radius R_1 in the second row of annuli adjacent to the line defect based on the W1.1 APCW (*i.e.* $w = 1.1*\sqrt{3}\,a$), while the inner radii were maintained at $r = 0.21a$. Figure 3(a) shows the calculated dispersion for various R_1 values. When R_1 increased from $0.32a$ to $0.39a$, the dispersion curves moved toward higher frequencies, and we realized that when R_1 was near $0.37a$ or beyond, the flat-band region emerged in the dispersion diagram. Figure 3(b) shows the curve of the group index corresponding to the waveguide modes in Fig. 3(a). Bands with constant group indices appeared in three curves for $R_1 = 0.37a$, $0.38a$, and $0.39a$.

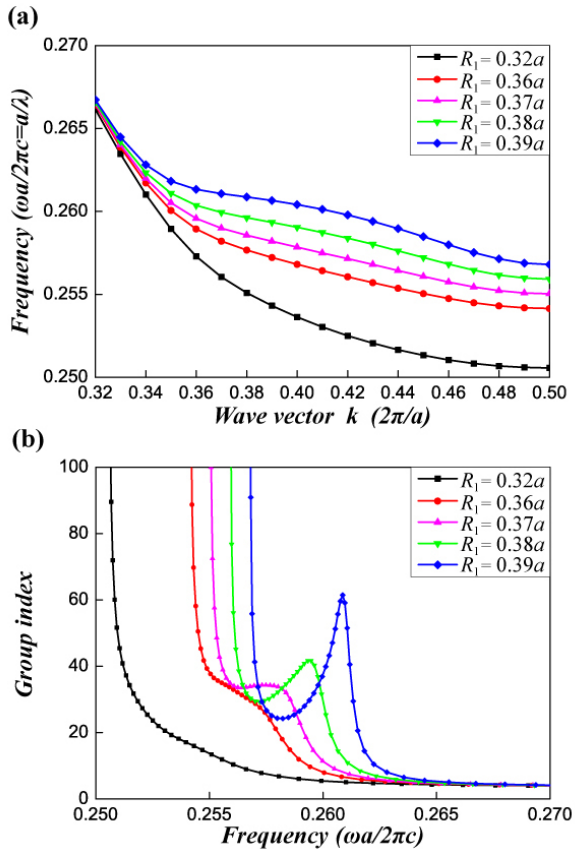

FIG. 3. (a) Dispersion diagram and (b) group-index curve for the alteration of the outer radius (R_1) of the second row of the annular air holes adjacent to the line defect.

Inspecting Fig. 3(a) again, we found that with increasing R_1 the dispersion curve had a faster blue shift in the region around $k = 0.4$ ($2\pi/a$) than the other region of the same dispersion curve. Therefore, the regions with constant group indices in Fig. 3(b) slowly changed from chairlike to U-shaped, which resulted in a smaller group index and a narrower bandwidth for slow light.

The normalized delay-bandwidth product (NDBP), a comprehensive index for evaluating the slow-light performance of an APCW, can be calculated by [23, 24]

$$NDBP = \overline{n_g} \times \left(\frac{\Delta\omega}{\omega_0}\right), \tag{1}$$

where $\overline{n_g}$ and $\Delta\omega/\omega_0$ are the average group index and the normalized bandwidth in the slow-light region respectively. The criterion for a worthy region of n_g can be explained as

$$\overline{n_g} = \int_{\omega-\frac{\Delta\omega}{2}}^{\omega+\frac{\Delta\omega}{2}} n_g(\omega) \times \frac{d\omega}{\Delta\omega}. \tag{2}$$

Usually the region of dispersion in relation to group index values within $\overline{n_g} \pm 10\%$ [5, 25] can be defined as an acceptable region for slow light applications.

Applying the above criterion, the group indices corresponding to $R_1 = 0.37a$, $0.38a$, and $0.39a$ were 36, 33.5, and 27.3, and the NDBP values were 0.387, 0.307, and 0.221 respectively. These decreasing NDBP values imply that it was not a wise choice to improve the slow-light performance by increasing R_1 based on $0.39a$.

Next, to improve the dispersion, optofluid infiltrations with different refractive indices n_f were applied to the second row of annuli adjacent to the line defect, for $R_1 = 0.37a$ and $0.38a$. The dispersion curves and group-index curves for two cases are shown in Figs. 4 and 5 respectively. The corresponding NDBP values are listed in Table 1.

As can be seen in Fig. 4(a), for $R_1 = 0.37a$, by increasing n_f, all of the APCW modes shifted to lower frequencies. However, since the rear portion of each curve approaching the edge of Brillouin zone was affected to a greater degree than the front portion, the bandwidth of the flat bands gradually widened, while the group indices gradually diminished. Fortunately, the areas with constant group indices in Fig. 4(b) maintained chairlike shapes for different n_f values. Therefore, the NDBP values stayed larger than 0.387 when n_f increased from 1 to 2.1, and the best NDBP value of 0.446 was achieved by infiltrating an optofluid with $n_f = 1.65$.

Then we turned to the case of $R_1 = 0.38a$. As shown in Fig. 5(a), the downward behavior of the curves is almost the same as that shown in Fig. 4(a). Hence, larger bandwidths and smaller group indexes occurred for bigger n_f values. However, in contrast to Fig. 4(b), the areas with constant group indices in Fig. 5(b) slowly changed from

being U-shaped to chairlike with increasing n_f, and the inflection point occured at $n_f = 1.95$. Because the chairlike type was more advantageous for obtaining a broad bandwidth, the NDBP values for $n_f = 1.95$ and $n_f = 2.1$, seen in Table 1, increased significantly compared to the cases with smaller n_f values, and the highest NDBP value of 0.502 was obtained at $n_f = 1.95$. Although the areas with constant group indices in Fig. 4(b) maintained a chairlike shape,

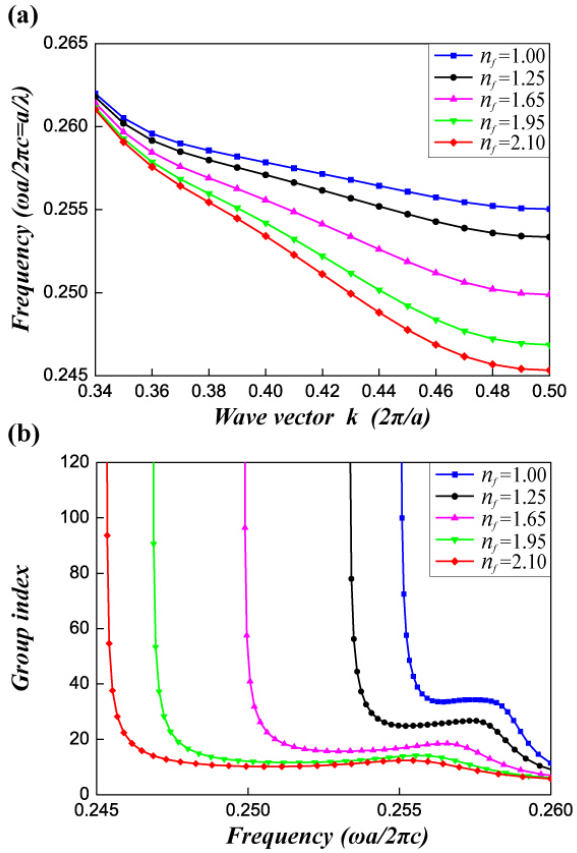

FIG. 4. (a) Dispersion diagram and (b) group-index curve for the different optofluid infiltrations into the second annular air hole row adjacent to the line defect with $R_1 = 0.37a$.

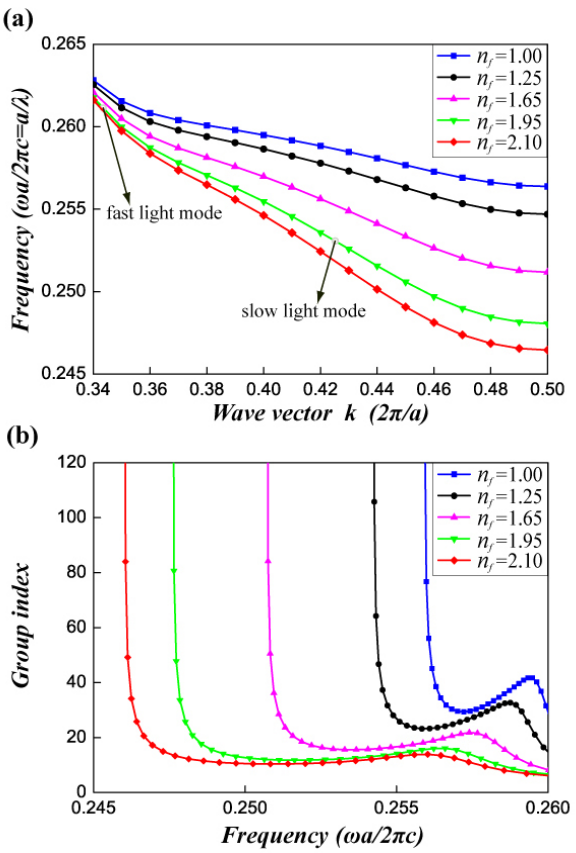

FIG. 5. (a) Dispersion diagram and (b) group-index curve for the different optofluid infiltrations into the second annular air hole row adjacent to the line defect with $R_1 = 0.38a$.

TABLE 1. Details of the group indices and the corresponding GVD, flat band's center wavelength λ_c, bandwidth $\Delta\lambda$, and NDBP for infiltrating different optofluids into the second row of annular air holes adjacent to the line defect

R_1	n_f	$\overline{n_g}$	GVD (ps^2/km)	Flat band		
				λ_c (nm)	$\Delta\lambda$ (nm)	NDBP
0.37a	1.00	36.0	10^5	1557.5	16.7	0.387
	1.25	28..0	10^5	1564.0	23.9	0.426
	1.65	18.0	10^5	1573.9	39.0	0.446
	1.95	14.5	10^5	1581.0	53.3	0.444
	2.10	11.7	10^5	1589.4	59.7	0.439
0.38a	1.00	33.5	10^5	1553.5	14.2	0.307
	1.25	26.5	10^5	1560.7	20.7	0.352
	1.65	17.9	10^5	1574.8	29.8	0.338
	1.95	13.6	10^5	1580.2	58.4	0.502
	2.10	11.9	10^5	1585.1	66.0	0.495

thanks to the wider bandwidth, the best NDBP value for $R_1 = 0.38a$ was larger than the best value for $R_1 = 0.37a$.

To illustrate the advantages of APCs over normal PCs in slow-light dispersion engineering, we compared the results of our current work to the previously reported results proposed by line-defect PCWs hosted in 2D air-hole or rod PCs. Our best NDBP value of 0.502 was higher than the results reported in Ref. [26] (NDBP = 0.48), Ref. [7] (NDBP = 0.465), and Ref. [12] (NDBP = 0.469).

As shown in Fig. 5(a), it can be found that in the same dispersion curve there are two regions where the slopes of the curves differ greatly. One region has a larger slope, because the corresponding group index is small, resulting in a large group velocity, called a *fast-light mode*. The other region with a smaller slope corresponds to a larger group index, and the group velocity is smaller; this region is called a *slow-light mode*. For further investigation, we selected two frequencies ($\omega_1 = 0.261$ ($2\pi c/a$) and $\omega_2 = 0.253$ ($2\pi c/a$)) in two regions in the dispersion curve of the APCW with $R_1 = 0.38a$ and $n_f = 1.95$ for modal-field-distribution simulation, using the finite-different time-domain (FDTD) method with a boundary treatment of perfectly matched layers. The fast-light and slow-light modes were excited by narrow-pulse sources ($\Delta\omega/\omega_0 = 1/200$) centered at 0.261 ($2\pi c/a$) and 0.253 ($2\pi c/a$) respectively. Figures 6(a) and 6(b) illustrate the screenshots of the stable field distribution with only two periods. For the longitudinal modal field distribution, the fast-light mode was more concentrated in the center of the waveguide, while the slow-light mode was extended more on the upper and lower sides. For the lateral field distribution, the slow-light mode showed more obvious mode compression and local field enhancement than the fast-light mode. It should be noted that the high-energy distribution of the oscillation period in the slow-light mode was much larger than in the fast-light mode, and the energy of the center was much larger than the center of the oscillation period of the fast-light mode.

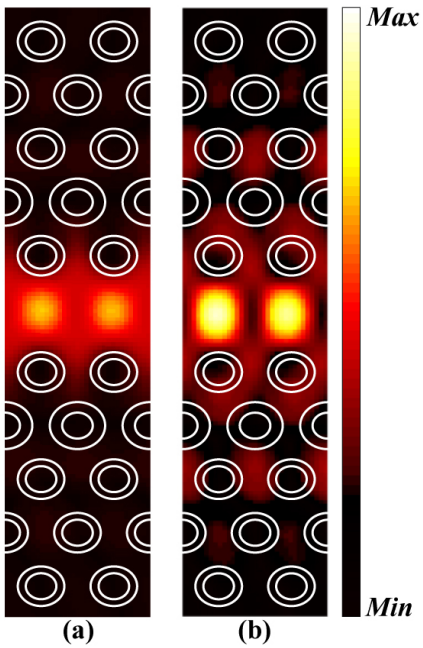

FIG. 6. Modal field distribution of the APCW with $R_1 = 0.38a$ and $n_f = 1.95$ for (a) fast-light mode and (b) slow-light mode.

Another important issue for slow-light devices is group-velocity dispersion (GVD), which causes pulse broadening and signal distortion [24]. The GVD, calculated by evaluating $\partial^2 k/\partial\omega^2$, is plotted in Fig. 7 for $R_1 = 0.38a$ and $n_f = 1.95$. To show the low-GVD advantage, the GVD was on the order of $10^5 (ps^2/km)$ in the slow-light region seen in Fig. 5(b), which was extremely small compared to those in Refs. [1], [4], and [15].

To verify the PWE results, numerical simulations were performed using the two-dimensional FDTD method with a boundary treatment of perfectly matched layers. In the simulation, we studied the transmission characteristics of an optical pulse in the infiltrated waveguide of Fig. 5 with $R_1 = 0.38a$ and $n_f = 1.95$. The transmission length was $100a$. The Gaussian-pulse source was centered at 0.253 ($2\pi c/a$) with a full width at half maximum (FWHM) of $\Delta\omega/\omega_0 = 1/30$. The average group index was calculated by

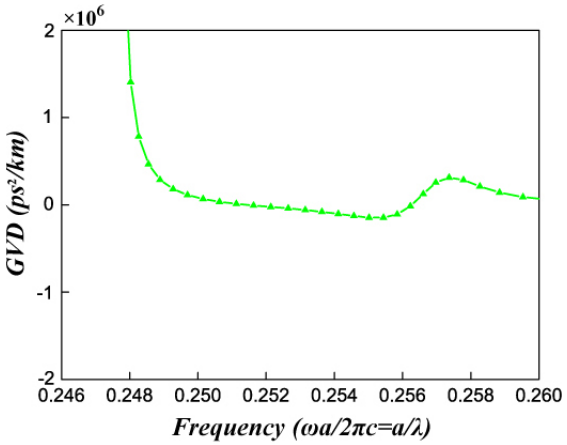

FIG. 7. Group-velocity dispersion (GVD) relationship calculated for an APCW with $R_1 = 0.38a$ and $n_f = 1.95$.

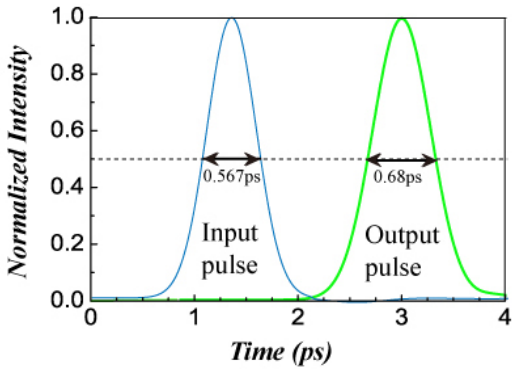

FIG. 8. Optical-pulse profile in the time domain, when it was propagating through the APCW with $\overline{n_g} = 13.6$.

the formula $\overline{n_g} = c\Delta t/L$, where Δt and L are the delay time between input and output pulses and the propagation length respectively. We considered the case for $\overline{n_g} = 13.6$. Figure 8 shows the normalized intensity in two monitors that were placed at the input and output ports of the waveguide. As illustrated, the peaks of the normalized field amplitude were observed at the input and output monitors at 1.3 ps and 3.01 ps respectively. Therefore, the time delay between the input pulse and the output pulse was equal to $\Delta t = 2.71 ps$. Consequently, the average group index could be calculated using the formula $\overline{n_g} = \Delta t \times c/100a = 12.75$, which agreed well with the PWE simulation. Furthermore, the FWHM of the injected pulse was distorted from 0.567 ps to 0.68 ps over the $100a$ propagation length. In other words, the relative pulse distortion was obtained as 0.6% per micrometer, which confirmed the low dispersion of the proposed waveguide.

III. SUMMARY

In summary, we investigated the slow light in a line-defect APCW. By altering the outer radius of the second row of the annular air holes adjacent to the center of the waveguide, and selectively injecting optoliquid as a post-processing method, high-performance slow light with a wide bandwidth of 58.4 nm, large NDBP value of 0.502, and low GVD of 10^5 (ps^2/km) could be obtained in the optical-communication window for a silicon-on-insulator structure. Our numerical results demonstrate that this approach allows researchers to exploit the proposed structure for ultracompact low-dispersion devices in the slow-light regime. Admittedly, the current work does not provide an exhaustive parameter search. Other APCW geometries might provide better performance.

ACKNOWLEDGMENT

Project supported by the Natural Science Foundation of China (No. 61605087, No. 61704083), the Natural Science Foundation of Jiangsu Province (No. BK20160881), and the Jiangsu Government Scholarship for Overseas Studies (JS-2017-021).

REFERENCES

1. H. Li, J. Wang, H. Lin, L. Xu, W. Xu, R. Wang, Y. Song, and D. Zhu, "Amplification of fluorescent contrast by photonic crystals in optical storage," Adv. Mater. **22**, 1237-1241 (2010).
2. J. Adachi, N. Ishikura, H. Sasaki, and T. Baba, "Wide range tuning of slow light pulse in SOI photonic crystal coupled waveguide via folded chirping," IEEE J. Sel. Top. Quantum Electron. **16**, 192-199 (2010).
3. S. Bakhshi, M. K. Moravvej-Farshi, and M. Ebnali-Heidari, "Design of an ultracompact low-power all-optical modulator by means of dispersion engineered slow light regime in a photonic crystal Mach-Zehnder interferometer," Appl. Opt. **51**, 2687-2692 (2012).
4. A. Rostami, A. Haddadpour, F. Nazari, and H. Alipour, "Proposal for an ultracompact tunable wavelength-division-multiplexing optical filter based on quasi-2D photonic crystals," J. Opt. **12**, 015405 (2010).
5. S. A. Schulz, L. O'Faolain, D. M. Beggs, T. P. White, and A. Melloni, T. F. Krauss, "Dispersion engineered slow light in photonic crystals: a comparison," J. Opt. **12**, 104004 (2010).
6. M. Ebnali-Heidari, C. Grillet, C. Monat, and B. J. Eggleton, "Dispersion engineering of slow light photonic crystal waveguides using microfluidic infiltration," Opt. Express **17**, 1628-1635 (2009).
7. A. Hocini, M. Maache, and D. Khedrouche, "Wideband and low dispersion slow light by altering the geometry of a photonic crystal waveguide," Opt. Commun. **427**, 396-404 (2018).
8. H. Kurt, K. Üstün, and L. Ayas, "Study of different spectral regions and delay bandwidth relation in slow light photonic crystal waveguides," Opt. Express **18**, 26965-26977 (2010).
9. J. Li, T. P. White, L. O'Faolain, A. Gomez-Iglesias, and T. F. Krauss, "Systematic design of flat band slow light in photonic crystal waveguides," Opt. Express **16**, 6227-6232 (2008).
10. J. Tang, T. Wang, X. Li, B. Wang, C. Dong, L. Gao, B. Liu, Y. He, and W. Yan, "Wideband and low dispersion slow light in lattice-shifted photonic crystal waveguides," J. Lightwave Technol. **31**, 3188-3194 (2013).
11. M. A. Mansouri-Birjandi, M. Janfaza, and A. Tavousi, "Flat-band slow light in a photonic crystal slab waveguide by vertical geometry adjustment and selective infiltration of optofluidics," J. Electron. Mater. **46**, 6528-6534 (2017).
12. M. Pourmand, A. Karimkhani, and F. Nazari, "Wideband and low-dispersion engineered slow light using liquid infiltration of a modified photonic crystal waveguide," Appl. Opt. **55**, 10060-10066 (2016).
13. A. Khodamohammadi, H. Khoshsima, V. Fallahi, and M. Sahrai, "Wideband slab photonic crystal waveguides for slow light using differential optofluidic infiltration," Appl. Opt. **54**, 1002-1009 (2015).
14. S. Pu, S. Dong, and J. Huang, "Tunable slow light based on magnetic-fluid-infiltrated photonic crystal waveguides," J. Opt. **16**, 045102 (2014).
15. H. Kurt and D. S. Citrin, "Annular photonic crystals," Opt. Express **13**, 10316-10326 (2005).
16. J. Hou, D. S. Citrin, H. Wu, D. Gao, and Z. Zhou, "Enhanced bandgap in annular photonic-crystal silicon-on-insulator asymmetric slabs," Opt. Lett. **36**, 2263-2265 (2011).
17. H. Wu, D. S. Citrin, L. Y. Jiang, and X. Y. Li, "Polarization-independent slow light in annular photonic crystals," Appl. Phys. Lett. **102**, 141112 (2013).
18. H. Wu and F. Li, "Negative-refraction effect for both TE and TM polarizations in two-dimensional annular photonic crystals," Curr. Opt. Photon. **2**, 47-52 (2018).
19. M. Qiu, "Effective index method for heterostructure-slab-waveguide-based two-dimensional photonic crystals," Appl. Phys. Lett. **81**, 1163-1165 (2002).

20. G. Hocker and W. K. Burns, "Mode dispersion in diffused channel waveguides by the effective index method," Appl. Opt. **16**, 113-118 (1977).
21. S. A. Schulz, A. H. K. Park, I. D. Leon, J. Upham, and R. W. Boyd, "Beyond the effective index method: improved accuracy for 2D simulations of photonic crystal waveguides," J. Opt. **17**, 075006 (2015).
22. A. Cicek and B. Ulug, "Polarization-independent waveguiding with annular photonic crystals," Opt. Express **17**, 18381-18386 (2009).
23. T. Baba, "Slow light in photonic crystals," Nat. Photonics **2**, 465-473 (2008).
24. J. Ma and C. Jiang, "Demonstration of ultraslow modes in asymmetric line-defect photonic crystal waveguides," IEEE Photon. Technol. Lett. **20**, 1237-1239 (2008).
25. M. D. Settle, R. J. P. Engelen, M. Salib, A. Michaeli, L. Kuipers, and T. F. Krauss, "Flatband slow light in photonic crystals featuring spatial pulse compression and terahertz bandwidth," Opt. Express **15**, 219-226 (2007).
26. S. Elshahat, K. Khan, A. Yadav, L. Bibbo, and Z. Ouyang, "Slow-light transmission with high group index and large normalized delay bandwidth product through successive defect rods on intrinsic photonic crystal waveguide," Opt. Commun. **418**, 73-79 (2018).